Assessing The Repeatability of Multi-Frequency Multi-Layer Brain Network Topologies Across Alternative Researcher's Choice Paths

Stavros I. Dimitriadis[1-6]*

[1] Integrative Neuroimaging Lab, 55133, Thessaloniki, Greece

[2] Cardiff University Brain Research Imaging Centre (CUBRIC), School of Psychology, College of Biomedical and Life Sciences, Cardiff University, CF24 4HQ, Cardiff, Wales, United Kingdom

[3] Neuroinformatics Group, Cardiff University Brain Research Imaging Centre (CUBRIC), School of Psychology, College of Biomedical and Life Sciences, CF24 4HQ, Cardiff, Wales, United Kingdom

[4] Division of Psychological Medicine and Clinical Neurosciences, School of Medicine, College of Biomedical and Life Sciences, Cardiff University, CF24 4HQ, Cardiff, Wales, United Kingdom

[5] Neuroscience and Mental Health Research Institute, School of Medicine, College of Biomedical and Life Sciences, Cardiff University, CF24 4HQ, Cardiff, Wales, United Kingdom

[6] MRC Centre for Neuropsychiatric Genetics and Genomics, School of Medicine, College of Biomedical and Life Sciences, Cardiff University, CF24 4HQ, Cardiff, Wales, United Kingdom

* corresponding author: Dr.Stavros I. Dimitriadis

Email: stidimitriadis@gmail.com / DimitriadisS@cardiff.ac.uk

Abstract—There is a growing interest in the neuroscience community on the advantages of multimodal neuroimaging modalities. Functional and structural interactions between brain areas can be represented as a network (graph) allowing us to employ graph-theoretic tools in multiple research directions. Researchers usually treated brain networks acquired from different modalities or different frequencies separately. However, there is strong evidence that these networks share complementary information while their interdependencies could reveal novel findings. For this purpose, neuroscientists adopt multilayer networks, which can be described mathematically as an extension of trivial single-layer networks. Multilayer networks have become popular in neuroscience due to their advantage to integrate different sources of information. We can incorporate this information from different modalities (multi-modal case), from different frequencies (multi-frequency case), or a single modality following a dynamic functional connectivity analysis (multi-layer,dynamic case). Researchers already used multi-layer networks to model brain disorders, to detect key hubs related to a specific function, to reveal structural-functional relationships, and to define more precise connectomic biomarkers related to brain disorders. However, the construction of a multilayer network depends on the selection of multiple preprocessing steps that can affect the final network topology. Here, we analyzed the fMRI dataset from a single human performing scanning over a period of 18 months (84 scans in total). We focused on assessing the reproducibility of multi-frequency multilayer topologies exploring the effect of two filtering methods for extracting frequencies from BOLD activity, three connectivity estimators, with or without a topological filtering scheme, and two spatial scales. Finally, we untangled specific combinations of researchers' choices that yield repeatable topologies, giving us the chance to recommend best practices over consistent topologies.

Index Terms—Functional connectivity; Network Topologies; Brain Connectivity; Multilayer networks; Test-Retest Study; Reproducibility ; Topological Filtering

I. INTRODUCTION

New developments in multimodal neuroimaging provide novel directions for measuring structural (anatomical) and functional connectivity (Tulay et al., 2019). These novel developments boost the emergence of brain connectivity (Sporns, 2011). An association exists between behavior and cognition and the brain's large-scale neuronal activity across spatially distributed brain areas (Alderson et al., 2020; Mišić and Sporns, 2016). Structural and functional connections between spatially

distributed brain areas are recognized as the key element of cognitive functions and behavioral repertoire (Mišić and Sporns, 2016; Smith et al., 2015). The progress of noninvasive imaging techniques has provided us with network maps of structural connections (anatomical) between neuronal elements (Sporns, 2014), and the simultaneous acquisition of dynamic brain activity (functional) (Loued-Khenissi et al., 2018). The brain is a complex system that can be described as a network (graph) where brain areas are the nodes and their links represent the functional and structural interactions between brain areas (Stam, 2014). The modeling of the brain as a network with any type of neuroimaging modality opens new avenues of graph-theoretic approaches and methods in multiple research directions (Bassett and Sporns, 2017).

Network or graph theory has been successfully applied to any neuroimaging modality across many, for example, functional magnetic resonance imaging (fMRI) (Lv et al., 2018), magnetoencephalography (MEG) (Pusil et al., 2019), electroencephalography (EEG) (Maturana-Candelas et al., 2019), diffusion magnetic resonance imaging (dMRI) (Messaritaki et al., 2019), and structural covariance (Carmon et al., 2020). Network theory enables us to simultaneously characterize the spatial organization (network topology) and the strength of any type (either structural or functional) connections (Bertolero and Bassett, 2020). Various network metrics that describe nodal (local) and global network characteristics like segregation, integration, (Rubinov and Sporns, 2010), and modularity (Sporns and Betzel, 2016) have been demonstrated their ability to describe quantitatively brain networks in various scientific pathways like in brain diseases (Crossley et al., 2014) and to discriminate brain states while subjects performing cognitive tasks (Braun et al., 2015).

The success of complex network theory in uncovering the key mechanisms of the human brain organization is limited by the use of single-later brain networks that capture only a single type of interaction (De Domenico, 2017). Functional neuroimaging modalities like MEG, EEG, and fMRI can capture brain activity across multiple frequencies and experimental time and it is important to explore the full spectrum (De Domenico et al., 2016; Dimitriadis et al., 2018a; Naro et al., 2021). In contrast, structural neuroimaging modalities such as diffusion-weighted imaging (DWI) measure the presence and strength of physical, anatomical connections between the various brain areas (Garcés et al., 2016). The necessity of taking

advantage of the increasing large multimodal open dataset repositories (Eickhoff et al., 2016) leads to the search for a new type of complex network that can encapsulate functional interactions across multiple frequency scales (multi-frequency case), across experimental time (multi-layer dynamic case), and across modalities (multi-modal case). However, trivial complex networks cannot provide neuroscientists with a mathematical framework to model all the existing interactions across frequencies, time, and modalities.

To present a solution to all the aforementioned challenges, recent research articles in network neuroscience have started to investigate the employment of multilayer networks. A multilayer network enables the integration of the information from single-layer networks with the incorporation of interconnected layers that connect these networks (Joseph et al., 2014). Into these current trends, recent research directions in network neuroscience have begun to investigate the employment of multilayer networks to model the multiplex associations that traditional networks are not suited to capture (Boccaletti et al., 2014; De Domenico, 2017; Muldoon and Bassett, 2016; Van Mieghem, 2016). Last years, multilayer networks have been introduced to the network neuroscience field (Brookes et al., 2016; Buldú and Porter, 2018; Dimitriadis et al., 2018a; Tewarie et al., 2016; Yu et al., 2017), where different layers correspond to different frequency-dependent functional interactions or to networks derived from different modalities or to a specific snapshot of a dynamic functional connectivity network (Battiston et al., 2017).

In the present study, we will focus on multi-frequency multilayer networks, and it is important to mention an important aspect of the construction of this type of multilayer network. Previous neuroimaging studies reported important findings based on multi-frequency multilayer networks. However, the inter-layer connections between frequency-dependent layers were defined as pseudo-links between homologous brain areas between the layers. This practically means that the inter-layer networks involve artificial links that interconnect each node with its representation across layers (Guillon et al., 2017; Yu et al., 2017). However, a true multi-frequency multilayer network should involve also inter-frequency layers that tabulate the cross-frequency interactions between the studying frequencies (Brookes et al., 2016; De Domenico et al., 2016; Dimitriadis et al., 2018a; Tewarie et al., 2016; Williamson et al., 2021).

The spectral features of the resting-state BOLD fMRI (rs-fMRI) multi-ROI signal are of high significant interest (Kalcher et al., 2014). We discovered an alignment between the frequency spectrum within the bandwidth 0 - 0.25 Hz with biological brain mechanisms (Hocke et al., 2016 ; Golestani et al., 2015). Specific spectral content has been associated with both vascular and physiological processes ((Golestani et al., 2015) ; (Hocke et al., 2016) ; (Mark et al., 2015)) and also with derived brain-network connectivity measures (Nikolaou et al., 2016)). A few studies attempted to decompose resting-state BOLD activity with either wavelet decomposition (Zhang et al., 2016) and with adaptive filtering like empirical mode decomposition (EMD) (Yuen et al., 2019). Here, we will adopt both methods to decompose the rs-fMRI multi-ROI time series into its intrinsic brain frequencies in a data-driven manner.

A tremendous amount of neuroimaging research articles adopted resting-state fMRI to define reliable connectomic biomarkers for many brain disorders and diseases (Parkes et al., 2020). Research findings on multi-frequency multilayer networks at resting-state fMRI (rs-fMRI) are preliminary (De Domenico et al., 2016). In order to design reliable connectomic biomarkers from resting-state fMRI, a prerequisite is the test-retest repeatability of network topologies (Luppi and Stamatakis, 2021). The majority of rs-fMRI studies adopted multilayer networks to model dynamic functional connectivity interactions in many target disease groups attempting to design reliable connectomic biomarkers (dynamic case ; (Braun et al., 2015; Dimitriadis et al., 2021; Gifford et al., 2020; Muldoon and Bassett, 2016)). Here, we analyze an rs-fMRI dataset from a single human performing scanning with various modalities over a period of 18 months. The total number of scans was 100. Our main goal is to assess the reproducibility of multi-frequency multilayer network topologies investigating the effect of potential choices over a) the filtering method for extracting frequencies from BOLD activity (empirical mode decomposition (EMD) (Yuen et al., 2019) versus wavelet decomposition (Zhang et al., 2016), b) the adopted functional connectivity estimator (Pearson's correlation coefficient, mutual information, and distance correlation), c) the topological layout of the derived functional brain network (fully-weighted network versus a topological filtering scheme with orthogonal minimal spanning trees (OMST)) (Dimitriadis et al., 2017a, 2017b) approach, and d) the spatial scale of the functional brain network (the original based on the parcellation scheme versus a downsampled version based on well-known

subnetworks). We adopted portrait divergence (Bagrow and Bollt, 2019) as a proper distance metric to quantify the network topology similarity between every pair of scans and across every set of the aforementioned preprocessing steps (2x3x2x2 = 24 distinct pipelines in total).

The rest of the paper is organized as follows: Section 2 describes the adopted dataset and the proposed preprocessing framework across multiple levels of choices. Section 3 is devoted to the results of the present study and, finally, section 4 discusses our findings giving instructions to the researchers while presenting the limitations of the current study.

II. MATERIALS AND METHODS

A. Resting-State fMRI (rs-fMRI)

Rs-fMRI was performed in 100 scans throughout the data collection period (89 in the production phase), using a multi-band EPI sequence (TR=1.16 ms, TE=30 ms, flip angle=63 degrees (the Ernst angle for the grey matter), voxel size=2.4 × 2.4 × 2 mm, distance factor=20%, 68 slices, oriented 30 degrees back from AC/PC, 96 × 96 matrix, 230 mm FOV, MB factor=4, 10:00 scan length). After session no.27, the number of slices was changed to 64 due to an update to the multi-band sequence that increased the minimum TR beyond 1.16 for 68 slices. Finally, 84 sessions were included in the analysis due to the low signal-to-noise ratio (SNR) for 16 sessions. For further details, an interesting read can see the original article describing this dataset (Poldrack et al., 2015). The dataset included ten 10-min runs of eyes-closed resting-state data and ten 10-min runs of eyes-open resting-state data. Here, we analyzed only the eyes-closed resting-open resting-state recordings. This famous dataset is called MyConnectome and one can test-retest the reproducibility over a long period of time that is absent in other test-retest studies.

B. Functional MRI preprocessing

For further details of the preprocessing steps of the rs-fMRI recordings, one can read the original paper presented the myConnectome dataset (Poldrack et al., 2015). The parcellation procedures lead to 630 parcels (ROIs).

C. Construction of Multi-frequency Multilayer Networks

Node definition:

We are defined as nodes in the multilayer network, every ROI characterized by a specific frequency content. In our study, we will decompose every ROI-based brain activity into four basic frequencies (see next section). This practically means that the size of our multilayer network will be: {4 x 630} x {4 x 630} = 2520 x 2520. This multilayer network will tabulate both the within and between frequencies coupling across every pair of ROIs. In multi-frequency multilayer networks, a node is defined as a frequency-dependent brain activity of every ROI.

Extracting of brain frequencies:

We extract wavelet coefficients for the first four wavelet scales, which correspond to the frequency ranges 0.125~0.25 Hz (Scale 1), 0.06~0.125 Hz (Scale 2), 0.03~0.06 Hz (Scale 3), and 0.015~0.03 Hz (Scale 4) (Zhang et al., 2016). Here, we adopted the maximum overlap discrete wavelet transform (MODWT), selecting the Daubechies family implemented with a wavelet length equal to 6.

Alternatively, we decompose resting-state BOLD activity into the related intrinsic mode functions (IMFs) with the empirical mode decomposition (EMD) (Yuen et al., 2019). We estimated the mean frequency of the Hilbert spectrum across time per brain area and IMF across scans.

We followed both decomposition methods first on the extracted averaged time-series per brain area for every scan across the 630 ROIs for Pearson's Correlation Coefficient (PC) and Mutual Information (MI) estimations, and secondly on the voxel time-series within every ROI per scan for Distance Correlation (DC) estimations. Fig.1 illustrates the decomposition with the two adopted methods of mean representative time series across voxels from the first two ROIs as presented in MyConnectome dataset. Fig.1A,B is dedicated to EMD and MODWT, respectively. We constructed multifrequency multilayer networks using the 8 in total time series (2 ROIs x 4 frequency subbands) and adopting the three connectivity estimators. The estimated network topologies for both decomposition methods are shown on the right side of each sub-figure. Blocks of connectivity strength within the 4 time series per ROI are tabulated within the main diagonal. The off-diagonal blocks tabulate connectivity strengths between the two sets of four-time series. Both PC and MI are estimated on the representative time series per ROI (shown in red) derived from

averaging the voxel-based time series (shown in blue). In contrast, DC is computed between two sets of voxel-based time series (shown in blue).

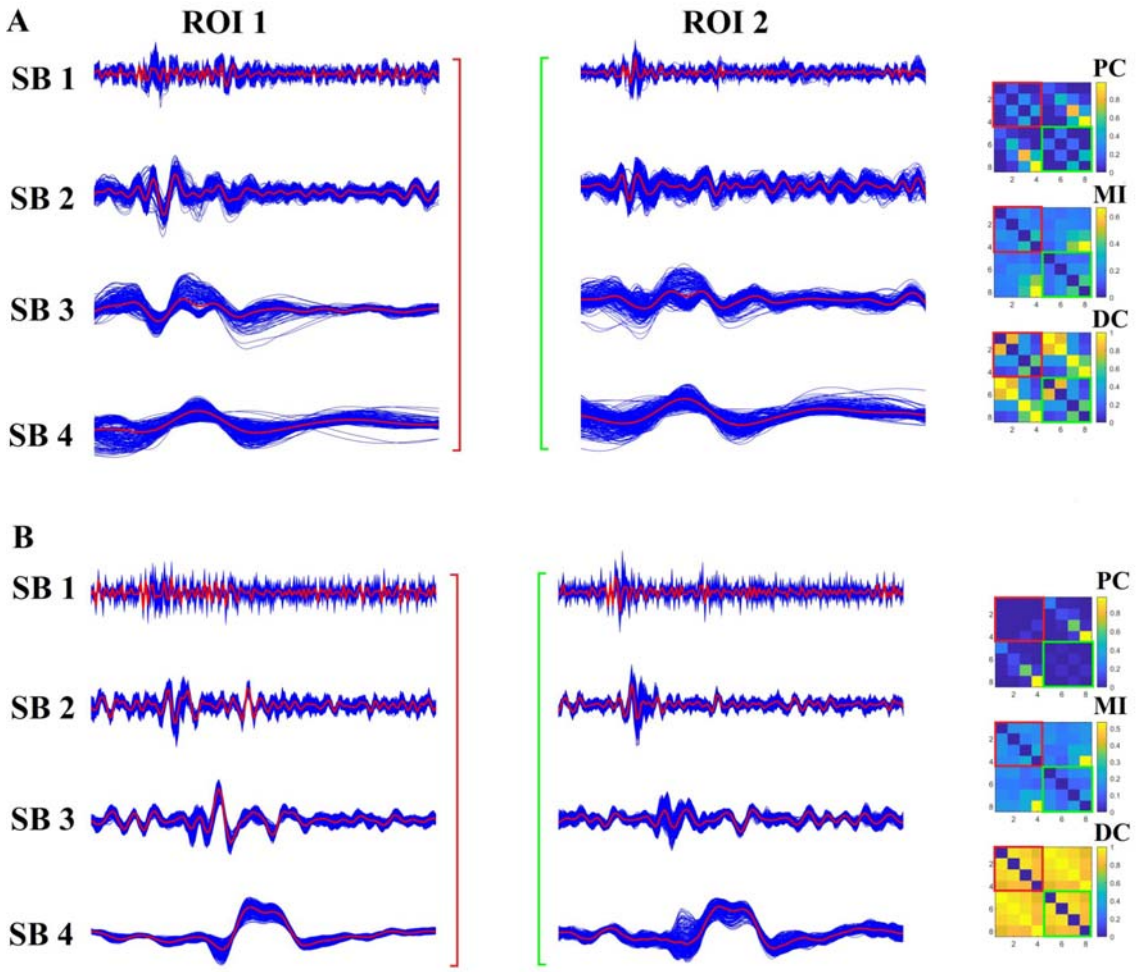

Figure 1. Decomposition of BOLD activity in frequency subbands with EMD (A) and MODWT (B).

We showed in blue the voxel-based time series for the first two ROIs from MyConnectome project using both decomposition methods. The averaged representative time series is shown in red. Network topologies tabulate the functional connectivity strength across the 8 time series (2 ROIs x 4-time series) with the three adopted connectivity estimators. Blocks within the main diagonal are color-coded to underline the functional interactions between the 4 time series per ROI. The off-diagonal blocks tabulate the functional connectivity strength of the two sets of 4-time series in a pair-wise fashion.

Functional Connectivity Estimators:

In the present study, we adopted three connectivity estimators that are divided into two groups. The first group involves the Pearson's Correlation Coefficient (PC), and the Mutual Information (MI). Both estimators can quantify the functional coupling strength between every pair of two frequency-dependent time-series derived as the ROI-averaged representative time-series. The second group involves the Distance Correlation (DC) metric that can quantify the correlation of two sets of frequency-dependent time-series corresponding to the voxel-based time-series of two ROIs.

We constructed a multilayer network whose ij^{th} elements are given by the three connectivity estimators with blocks in the main diagonal of size 630 x 630 corresponding to the four within-frequency functional connectivity networks and off-diagonal blocks of size 630 x 630 corresponding to every possible pair of the between-frequency functional connectivity networks (4x3/2=6 in total). The aforementioned procedure was followed for every single scan, filtering method, and connectivity estimator.

For each parcellation, the average denoised BOLD time-series across all voxels belonging to a given ROI were extracted. We considered three alternative ways of quantifying the interactions between regional BOLD signal time series.

Below, we defined the mathematical descriptions of the adopted connectivity estimators.

Pearson linear correlation:

First, we used Pearson correlation, whereby for each pair of nodes *i* and *j,* their functional connectivity strength FCS_{ij} was given by the Pearson correlation coefficient between the timecourses of *i* and *j*, over the full scanning length. We got the absolute Pearson's correlation values that bound the range of FCS within [0,1].

Mutual information (MI)

Second, we also used the mutual information *I,* which quantifies the interdependence between two random variables X and Y, and is defined as the average reduction in uncertainty about X when Y is given (or vice versa, since this quantity is symmetric):

$$I(X;Y) = H(X) + H(Y) - H(X,Y) = H(X) - H(X|Y) \quad (1)$$

With *H(X)* being the Shannon entropy of a variable X. Unlike Pearson correlation, mutual information considers both linear and nonlinear relationships. We normalized mutual information (MI) values by dividing the maximum value in the matrix-bound within [0,1].

Distance Correlation:

Third, we adopted for the very first time based on the authors' knowledge distance correlation as a proper functional connectivity estimator in functional brain network construction. This new test is based on an unbiased estimator of distance covariance, and the resulting t-test is unbiased for large sample sizes (> 30) (Székely and Rizzo, 2013). The combined p-value can be estimated analytically. Here, we adopted distance correlation to estimate the functional connectivity strength between pairs of tuples of voxel-based time series between every pair of ROIs.

Surrogate Null Models: Statistical Topological Filtering

Since the ground truth of the presence of true functional connections cannot be defined, the construction of surrogate data as a statistical framework is inevitable (Pereda et al., 2005; Schreiber and Schmitz, 2000). Surrogate time series must preserve specific properties of the original time series in order to be useful. These properties are the auto□covariance sequence, stationary cross□correlation, power spectral density, cross power spectral density, and amplitude distribution (Pereda et al., 2005; Schreiber and Schmitz, 2000; Zalesky et al., 2014). In the present study, we adopted two basic surrogate data methods: the first one produces surrogate data adopting the notion of the multivariate phase randomization (MVPR) (Prichard and Theiler, 1994), and the second is called multivariate autoregressive (MVAR) (Savva et al., 2019; Zalesky et al., 2014).

The MVPR method is first described for generating surrogate time series (Prichard and Theiler, 1994). Below, we described briefly the steps of producing the surrogate time series. Let $x = [x_1,x_2,...,x_n]$ denote the BOLD recordings from n=630 parcels each of these time series is composed of 518 time points and $X =[X_1,X_2,...,X_n]$ denote their discrete Fourier transform. Then, we generated a uniformly distributed random

phase ($\varphi = [\varphi_1,\varphi_2,...,\varphi_T]$), within the interval [0, 2π] and we further applied to each signal with the following equation: $X_k = X_k^{ei\varphi}$, k = 1,2,...,n. Practically, this transformation means that in the frequency domain, all our recorded signals are multiplied by the same uniformly random phase (Hindriks et al., 2016). Finally, we estimated the inverse Fourier transform and we got our first surrogate dataset. We repeated the same procedure 1,000 times producing 1,000 surrogate datasets for every scan.

MVAR models produce a set of signals described as a combination of both their own past and also the past of the entire set of signals in the multidimensional set (Prichard and Theiler, 1994). The polynomial order p defines the number of past signal values that are considered in the MVAR model. We selected the value of p based on the minimization of the Schwarz Bayesian Criterion (SBC) (Zalesky et al., 2014). Again, a total number of 1,000 randomized copies were created for each subject (Hindriks et al., 2016; Zalesky et al., 2014).

We applied both MVPR and MVAR on the original BOLD time series.

Surrogate Null Hypothesis

For every multifrequency multilayer network, we generated 1,000 surrogate multilayer networks based on both methods. Then, we assigned to every functional connection a *p*-value by estimating the proportion of surrogate connectivity values that were higher than the observed values (Theiler et al., 1992). To correct the effects of multiple comparisons, *p*-values were adjusted using the false discovery rate (FDR) method (Benjamini and Hochberg, 1995; Dimitriadis et al., 2015). A threshold of significance *q* was set such that the expected fraction of false positives was restricted to $q \leq 0.01$ (Dimitriadis, 2021; Dimitriadis et al., 2015). The whole procedure was repeated separately across filtering methods, connectivity estimators, and scans. Statistical topological filtering multifrequency multilayer networks were then fed to our data-driven topological filtering scheme called OMST.

Data-driven topological filtering scheme:

An important preprocessing step for brain networks is to topologically filter out the backbone of functional links across the whole network. Here, we adopted our data-driven technique called Orthogonal Minimal Spanning Trees (OMST) (Dimitriadis et al., 2017a, 2017b) for the very first time to topologically filter a multilayer network.

OMST (Dimitriadis et al., 2017a, 2017b) is a data-driven approach that optimizes the balance between global efficiency and the global-cost efficiency of the network which is defined as the global efficiency minus the cost. The cost is defined as the ratio of the sum of functional strength of the selected functional links versus the total sum of functional strength of all the pairs of functional links (fully-weighted version of the network). OMST can be described with the following steps : (1) at the first stage, the original MST is extracted consisting of N-1 functional links (where N denotes the total number of nodes) that connect all the nodes while simultaneously minimizing the average wiring cost. MST captures the main net of functional links where the major part of all pairs of shortest paths pass through. Global efficiency and global-cost efficiency are estimated for the 1st MST ; (2) Then, the N-1 functional links were removed from the network, and we searched for the 2nd MST which is orthogonal to the first. We added the 1st and 2nd MST to the network, and we again estimated the global efficiency and the global-cost efficiency ; (3) We repeated the same procedure until a global maximum is detected on the plot of global-cost efficiency versus the total cost. For further details, see the original articles (Dimitriadis et al., 2017a, 2017b). The OMST procedure produces sparse functional networks but denser than using only the first MST. Moreover, OMST method doesn't impose a-priori selected sparsity level across a cohort, and it produces highly reliable structural and functional networks compared to alternative topological filtering schemes (Dimitriadis et al., 2017c, 2018b; Messaritaki et al., 2019). Here, we analyzed fully-weighted multilayer networks and topologically filtered multilayer networks with OMST.

Network Scales:

In the present study, we constructed a multilayer network based on the parcellation scheme provided by the authors of MyConnectome project (Poldrack et al., 2015). The total number of ROIs as was already aforementioned was 630. Here, we explored the within and between frequency interactions across every pair of ROI for a total of four frequency bands as extracted with MODWT and EMD methods. This practically means that the size of our multilayer network will be equal: {4 x 630} x {4 x 630} = 2520 x 2520. Fig.2 visualizes an example of a multifrequency multilayer network constructed with the combination of EMD and PC. Fig.2A illustrates the fully-weighted multifrequency multilayer network while the OMST version of the multilayer network is depicted in Fig.2B. Simultaneously, as many researchers integrated their

findings into well-known resting-state networks, we decided to create a subnetwork multilayer network as follow: we computed the mean of pair-wise functional strength between ROIs that comprised each of the following thirteen cognitive networks as provided within the MyConnectome project (Poldrack et al., 2015). These subnetworks are Default Mode Network, Somatomotor, Ventral_Attention, Frontoparietal_1, Frontoparietal 2, Visual_1, Visual_2, Medial_Parietal, Parieto_occipital, Cingulo_opercular, Salience, Dorsal_Attention, and a final subnetwork that includes ROIs that are not classified to the twelve subnetworks. The final size of these subnetworks are equal to : {4 x 13} x {4 x 13} = 52 x 52. An example of a small-scale multilayer network is shown in Fig.3 for the combination of EMD and PD as in Fig.2.

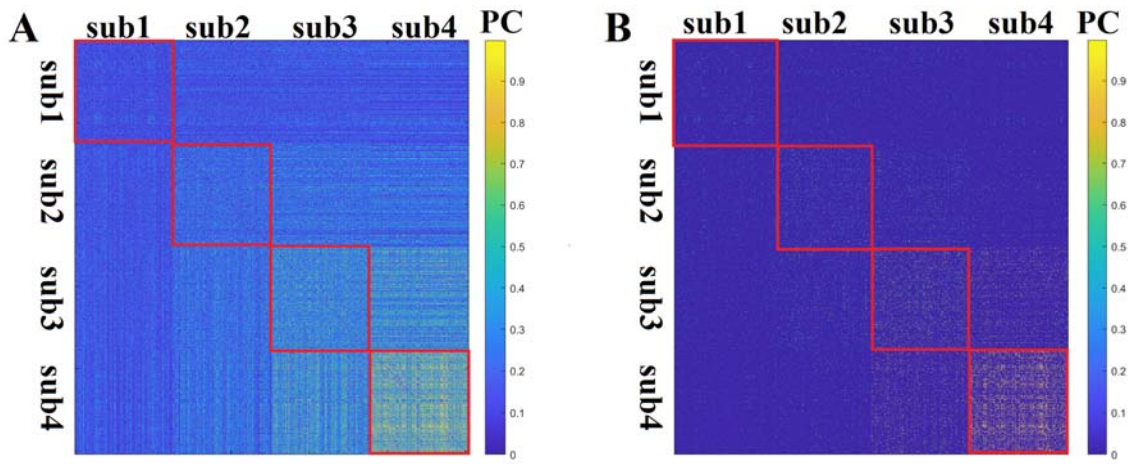

Figure 2. An example of a full-resolution multifrequency multilayer network from the 1st scan derived from the combination of EMD filtering technique and PC as a proper functional connectivity estimator.

A) A fully-weighted version of the multifrequency multilayer network

B) OMST version of the multifrequency multilayer network shown in A

In-diagonal red blocks underline the intra-frequency functional networks of size 630x630. Off-diagonal blocks refer to cross-frequency (inter-frequency) functional networks of the same size (**sub - subband**)

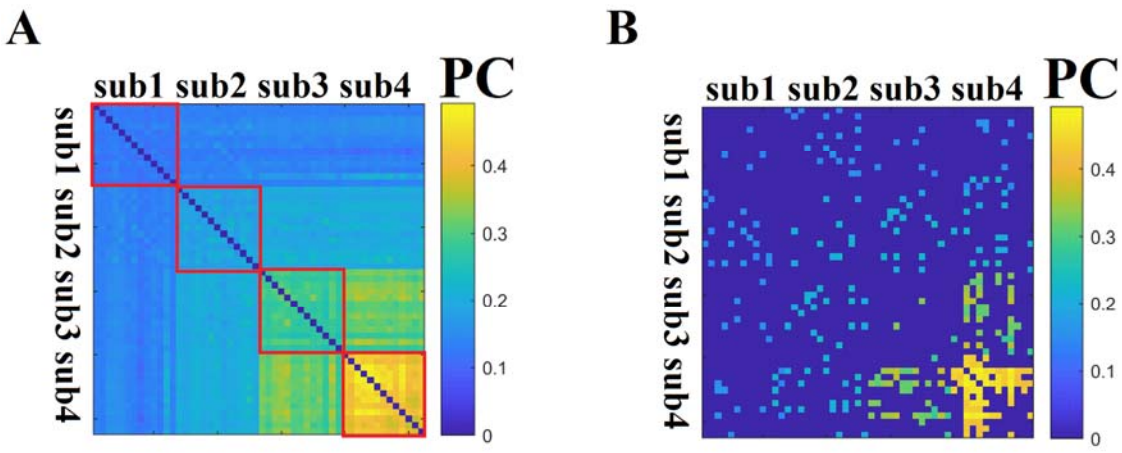

Figure 3. An example of a low-resolution multifrequency multilayer subnetwork from the 1st scan derived from the combination of EMD filtering technique and PC as a proper functional connectivity estimator. The size of this subnetwork is 52 x 52.

A) The fully-weighted low-resolution multifrequency multilayer subnetwork. In-diagonal red blocks underline the intra-frequency functional subnetworks of size 13x13. Off-diagonal blocks refer to cross-frequency (inter-frequency) functional subnetworks of the same size.

B) The OMST version of the low-resolution multifrequency multilayer subnetwork (**sub - subband**)

Topological Distance as Portrait Divergence:

To quantify the difference between network topologies, we used the recently developed Portrait Divergence (PDiv). The Portrait Divergence (PDiv) between two graphs G_1 and G_2 is the Jensen-Shannon divergence between their "network portraits", which encode the distribution of shortest paths of the two networks (Bagrow and Bollt, 2019). Specifically, the network portrait is a matrix B whose entry B_{lk}, $l = 0, 1, \ldots, d$ (with d being the graph diameter), $k = 0, 1, \ldots, N - 1$, is the number of nodes having k nodes at shortest-path distance l. For further details, an interested reader can read the original article describing this method (Bagrow and Bollt, 2019).

PDiv considerates all the scales of the topology within the networks from motifs to large-scale connectivity patterns and is not restricted to a single network property (Bagrow and Bollt, 2019).

For each scan, we obtained one brain network following each of the possible combinations of steps above (2x3x2x2 = 24 distinct pipelines in total).

For each pipeline, we then computed the PDiv between multilayer brain network topologies obtained from the single subject at different time points (scans). This procedure constructed a similarity matrix of size 84x84 (scans x scans) and tabulated the PDiv distance of the multilayer brain network topologies related to every scan in a pair-wise fashion. We finally estimated the mean PDiv across every

possible pair of 84 scans (84x83/2 = 3486 pairs) to characterize the quality of each of the 24 distinct pipelines. Fig.4 illustrates scan-to-scan pair-wise PDiv distances between every pair of multifrequency multilayer networks. The column on the right shows the sum of every row in the distance D matrix called ΣPDiv. This vector of size equal to the number of scans expresses the (dis)similarity of every single-scan multilayer network topology across the rest of the scan-related multilayer network topologies.

We set up a criterion of PDiV < 0.1 to characterize a pipeline as repeatable.

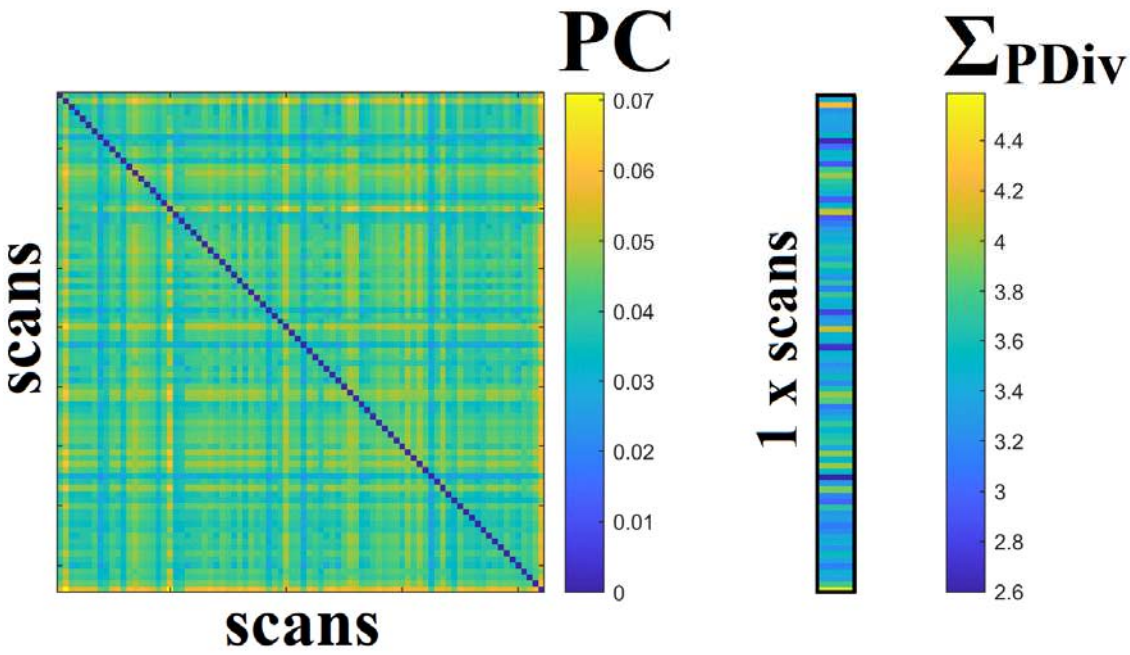

Figure 4. Scan-to-Scan pairwise topological PDiv distances between pairs of multifrequency multilayer networks. The column on the right shows the sum of every row in the distance D matrix called ΣPDiv. The size of this vector is equal to the number of scans.

Statistical Analysis:

Scan-averaged PDiv were estimated for each of the potential 24 distinct pipelines. To explore the effect of researcher choice at the four levels of preprocessing steps on the repeatability of multi-frequency multilayer topology, we followed an n-way ANOVA ($p < 0.05$). We performed two three-way ANOVA with repeated measures on three factors (filtering - connectivity estimator - topological layout), one in the atlas and one in the subnetworks space. As an input to the three-way ANOVA, we employed the 84 values produced by the sum of every row of the distance matrix as it was shown in Fig.4. The final p-values of every single preprocessing step and their interactions were adjusted for multiple comparisons.

III. RESULTS

Appropriate Surrogate Model for Statistical Filtering of Multilayer Networks

Produced surrogate time series must preserve specific properties of the original time series in order to be useful. Only surrogate BOLD time series produced by the MVPR model fulfilled the aforementioned prerequisites. MVAR failed to produce a useful surrogate BOLD time series. For that reason, MVPR was our single surrogate algorithmic choice and surrogate analysis was not involved in our main aim of how the researcher's choice may affect the repeatability of multifrequency multilayer brain network topologies.

Characteristic Intrinsic Frequency Modes for Resting-State BOLD Activity based on MODWT and EMD

We estimated characteristic frequency per representative ROI time series per scan. For the MODWT decomposition scheme, we adopted the *pwelch* method as provided by MATLAB. For the EMD decomposition scheme, we adopted the *hht* method as provided by MATLAB. We first averaged the characteristic frequency per ROI across scans and afterward, we got the mean and standard deviation across the number of ROIs. Table 1 summarizes the whole-brain averaged characteristic intrinsic frequency modes for resting-state BOLD activity extracted with both filtering schemes. It is evident that the mean frequency of subbands between the two filtering methods doesn't overlap.

Table 1. Whole-brain averaged intrinsic frequency modes for both MODWT and EMD filtering schemes

	Subband 1	**Subband 2**	**Subband 3**	**Subband 4**
MODWT	**0.21 ± 0.004**	**0.11 ± 0.004**	**0.049 ± 0.004**	**0.021 ± 0.004**
EMD	**0.27 ± 0.012**	**0.14 ± 0.011**	**0.072 ± 0.006**	**0.023 ± 0.003**

Researcher's Free Choice Preprocessing Paths May Affect the Repeatability of Multilayer Multifrequency Network Topologies

Results of three-way ANOVA with repeated measures on three factors (filtering - connectivity estimator - topological layout) in the atlas and subnetworks space revealed an effect on the repeatability of multilayer multifrequency topologies ($p < 0.05$; corrected for multiple comparisons; see Table 2 and 3). Fig.5 illustrates the across-scans PDIv values averaged and the relevant standard deviations per pipeline. It is important to mention here that repeatability is preserved in both the atlas and subnetworks spatial layout (PDiV < 0.1). PC and DC seem to produce more repeatable network topologies than MI (lower PDiV values) in both filtering methods and both spatial layouts with the only exception of the combination of MODWT- MI - SUBNETWORKS - OMST/FULLY-WEIGHTED (see the rightmost sub-area in Fig.5). In all the pipelines, OMST data-driven topological filtering method further improves the repeatability of multilayer network topologies (minimizing PDiV values). Another significant outcome of our study is that both filtering methods produce repeatable multilayer network topologies in both spatial scales. The only five exceptions (PDiV > 0.1) are the following: ATLAS - EMD - MI - OMST/FULLY-WEIGHTED, SUBNETWORKS - EMD - MI - FULLY-WEIGHTED and ATLAS - MODWT - MI - OMST/FULLY-WEIGHTED.

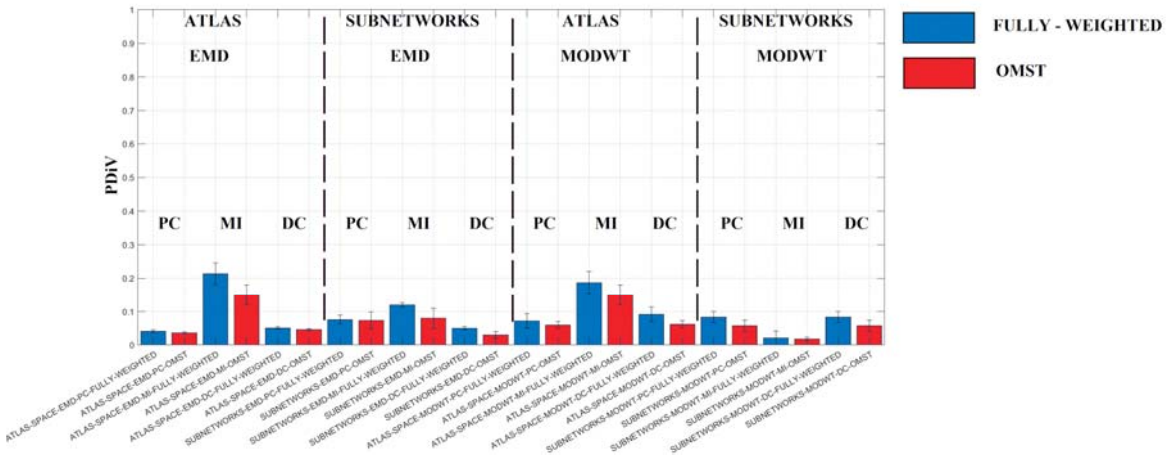

Figure 5. PDiV scan-averaged values across every possible pipeline (24 in total) among the four factors explored in our study

Table 2. Three-Way Analysis of Variance With Repeated Measures on Three Factors (Within-Subjects) Table based on Full Network Resolution Analysis

SOV	SS	df	MS	F	P	Conclusion
Between-Subjects	**0.278**	**83**				
Within-Subjects	**22.618**	**924**				
FiltM	**0.038**	**1**	**0.038**	**9.197**	**0.0032**	**S**
Error(FiltM)	**0.343**	**83**	**0.004**			
FCE	**12.944**	**2**	**6.472**	**1936.404**	**0.0000**	**S**
Error(FCE)	**0.555**	**166**	**0.003**			
NT	**1.462**	**1**	**1.462**	**396.851**	**0.0000**	**S**
Error(NT)	**0.306**	**83**	**0.004**			
FiltMxFCE	**1.645**	**2**	**0.822**	**205.859**	**0.0000**	**S**
Error(FiltM-FCE)	**0.663**	**166**	**0.004**			
FiltMxNT	**0.148**	**1**	**0.148**	**37.936**	**0.0000**	**S**
Error(FiltM-NT)	**0.323**	**83**	**0.004**			
FCExNT	**2.296**	**2**	**1.148**	**404.146**	**0.0000**	**S**

Error(FCE-NT)	**0.471**	**166**	**0.003**			
FiltMxFCExNT	**0.723**	**2**	**0.362**	**108.238**	**0.0000**	**S**
Error(FiltM-FCE-NT)	**0.555**	**166**	**0.003**			
Total	**22.749**	**1007**				

With a given significance level of: 0.05

The results are significant (S) or not significant (NS).

FiltM : filtering method (MODTW or EMD)

FCE : functional connectivity estimator (PC,MI,DC)

NT : Network topology (fully-weighted network vs OMST)

Table 3. Three-Way Analysis of Variance With Repeated Measures on Three Factors (Within-Subjects) Table based on Subnetwork Resolution Analysis

SOV	SS	df	MS	F	P	Conclusion
Between-Subjects	**0.077**	**83**				
Within-Subjects	**8.999**	**924**				
FiltM	**0.009**	**1**	**0.009**	**13.738**	**0.0004**	**S**
Error(FiltM)	**0.052**	**83**	**0.001**			

FCE	**0.603**	**2**	**0.302**	**671.013**	**0.0000**	**S**
Error(FCE)	**0.075**	**166**	**0.000**			
NT	**3.023**	**1**	**3.023**	**2645.330**	**0.0000**	**S**
Error(NT)	**0.095**	**83**	**0.001**			
FiltMxFCE	**0.340**	**2**	**0.170**	**481.421**	**0.0000**	**S**
Error(FiltM - FCE)	**0.059**	**166**	**0.000**			
FiltMxNT	**0.288**	**1**	**0.288**	**420.998**	**0.0000**	**S**
Error(FiltM - NT)	**0.057**	**83**	**0.001**			
FCExNT	**3.037**	**2**	**1.519**	**3318.529**	**0.0000**	**S**
Error(FCE-NT)	**0.076**	**166**	**0.000**			
FiltMxFCExNT	**0.928**	**2**	**0.464**	**1104.304**	**0.0000**	**S**
Error(FiltM-FCE-NT)	**0.070**	**166**	**0.000**			
Total	**8.788**	**1007**				

With a given significance level of: 0.05

The results are significant (S) or not significant (NS).

FiltM : filtering method (MODTW or EMD)

FCE : functional connectivity estimator (PC,MI,DC)

NT : Network topology (fully-weighted network vs OMST)

IV. DISCUSSION

A large amount of current neuroimaging research with fMRI is focused on harnessing repeatable brain network-based connectomic biomarkers related to both normal and abnormal brain function. However, this investigation involves a combination of arbitrary preprocessing choices (Korhonen et al., 2021). Test-retest repeatability is a prerequisite over the definition of repeatable connectomic biomarkers (Fornito et al., 2015; Hallquist and Hillary, 2019). Here, we explored for the very first time in the literature how different researcher's choices may affect the repeatability of multilayer multifrequency network topologies. We systematically investigated 24 unique pipelines from resting-state fMRI recordings acquired from 84 scans of a single subject (MyConnectome dataset ; (Poldrack et al., 2015)). Test-retest studies of resting-state fMRI single-layer brain networks focused on the reliability of graph metrics in various cohorts and in both short and long-term periods between scans (Andellini et al., 2015; Noble et al., 2017, 2019; Somandepalli et al., 2015; Song et al., 2012; Termenon et al., 2016; Wang et al., 2017 ; Somandepalli et al., 2015). However, the estimation of graph metrics derived from the network topology and the final conclusion regarding the reliability of these network metrics might differ from study to study due to the researcher's choice of which to represent and also due to their different nature. For the above reasons, our research focused on how the overall multilayer network topology quantified with PDiV measurement is affected on the 24 pipelines across the 84 scans.

We first investigated the quality of surrogate time series produced by two important methods, the MVAR and MVPR. Based on specific time-frequency criteria, we decided that MVPR is our unique algorithmic choice for the surrogate analysis and statistical topological filtering of the multilayer multifrequency networks.

To address the effect of three factors (topological filtering - connectivity estimator - topological layout) on the repeatability of multilayer multifrequency topologies, we repeated a three-way ANOVA in the atlas and subnetwork space. Our main finding is that repeatability (PDiV < 0.1) is preserved in both the atlas and subnetworks spatial layout. PC and DC produce more repeatable network topologies than MI (lower PDiV values) in both filtering methods and both spatial layouts with the only exception of the combination of MODWT- MI - SUBNETWORKS - OMST/FULLY-WEIGHTED. In

all pipelines, our OMST data-driven topological filtering method further improves the repeatability of multilayer network topologies (minimizing PDiV values). An interesting finding that deserves further consideration is that both filtering methods produce repeatable multilayer network topologies in both spatial scales. The only five out of twenty-four pipelines exceptions that lead to not repeatable topologies (PDiV > 0.1) are the following: ATLAS - EMD - MI - OMST/FULLY-WEIGHTED, SUBNETWORKS - EMD - MI - FULLY-WEIGHTED and ATLAS - MODWT - MI - OMST/FULLY-WEIGHTED.

It is important to mention here that five out of twenty-four pipelines include MI as a connectivity estimator. In addition, against the overall superiority of OMST compared to fully-weighted multilayer networks, two out of the five worst pipelines include OMST. This finding can be interpreted in conjunction with three-way ANOVA findings where the combination of processing choices matters and a single choice cannot guarantee the reproducibility of network topologies.

In the present study, we decided to decompose the BOLD signal with a well-known technique, the MODWT (Zhang et al., 2016) vs an adaptive filtering technique called EMD (Yuen et al., 2019). Our intention was to demonstrate how different filtering techniques of the BOLD signal can lead to repeatable multilayer multifrequency topologies as part of a common preprocessing pipeline. The mean frequency across the ROIs and scans of every frequency subband with both methods didn't overlap. This finding could be evidence of the complementary information encapsulated by the ROI-based time series extracted from both the filtering methods. This is definitely a statement that deserves further consideration in a multi-subject test-retest study.

Limitations

In particular, we did not explore potential differences between resting-state conditions (eyes-open vs eyes-closed vs naturalistic viewing) (Van Dijk et al., 2010; Wang et al., 2011), or the impact of scan duration and arousal state (Laumann et al., 2017). Similarly, we did not consider a wide number of alternative parcellation schemes in existence but we adopted the parcellation scheme proposed by the authors provided for free this dataset (Arslan et al., 2018; Eickhoff et al., 2018). Test-retest studies are the first step of a systematic evaluation of how alternative network processing steps can affect the repeatability of network topologies. We hope that the

proposed network topology construction framework will lead to more consistent analytic practices in the human network neuroscience of functional neuroimaging data.

Conclusions

In conclusion, our study provides an exploratory framework searching for the best multilayer multifrequency network construction pipelines across hundreds of candidates, with the aim of recovering a reliable brain network topology. Our findings support that only the combination of several specific processing steps can guarantee the repeatability of multilayer network topologies. We untangled that every choice across the adopted processing steps matters and specific pipelines can produce similar network topologies over the period of eighteen months. Interestingly, alternative pipelines produce repeatable multilayer networks leading to the assumption that they share complementary information.

Acknowledgements

MRC grant MR/K004360/1 (Behavioural and Neurophysiological Effects of Schizophrenia Risk Genes: A Multi-locus, Pathway Based Approach) [SID] and by a MARIE-CURIE COFUND EU-UK Research Fellowship [SID].

Conflict of Interest

The authors declare that there is no conflict of interest regarding the publication of this article.

References

Alderson, T.H., Bokde, A.L.W., Kelso, J.A.S., Maguire, L., and Coyle, D. (2020). Metastable neural dynamics underlies cognitive performance across multiple behavioural paradigms. Hum. Brain Mapp. *41*, 3212–3234.

Andellini, M., Cannatà, V., Gazzellini, S., Bernardi, B., and Napolitano, A. (2015). Test-retest reliability of graph metrics of resting state MRI functional brain networks: A review. J. Neurosci. Methods *253*, 183–192.

Arslan, S., Ktena, S.I., Makropoulos, A., Robinson, E.C., Rueckert, D., and Parisot, S. (2018). Human brain mapping: A systematic comparison of parcellation methods for the human cerebral cortex. Neuroimage *170*, 5–30.

Bagrow, J.P., and Bollt, E.M. (2019). An information-theoretic, all-scales approach to comparing networks. Appl. Netw. Sci. *4*, 45.

Bassett, D.S., and Sporns, O. (2017). Network neuroscience. Nat. Neurosci. *20*, 353–364.

Battiston, F., Nicosia, V., Chavez, M., and Latora, V. (2017). Multilayer motif analysis of brain networks. Chaos *27*, 047404.

Benjamini, Y., and Hochberg, Y. (1995). Controlling the false discovery rate: a practical and powerful approach to multiple testing. Journal of the Royal Statistical Society: Series B (Methodological) *57*, 289–300.

Bertolero, M.A., and Bassett, D.S. (2020). On the nature of explanations offered by network science: A perspective from and for practicing neuroscientists. Top. Cogn. Sci. *12*, 1272–1293.

Boccaletti, S., Bianconi, G., Criado, R., Del Genio, C.I., Gómez-Gardeñes, J., Romance, M., Sendiña-Nadal, I., Wang, Z., and Zanin, M. (2014). The structure and dynamics of multilayer networks. Phys. Rep. *544*, 1–122.

Braun, U., Schäfer, A., Walter, H., Erk, S., Romanczuk-Seiferth, N., Haddad, L., Schweiger, J.I., Grimm, O., Heinz, A., Tost, H., et al. (2015). Dynamic reconfiguration of frontal brain networks during executive cognition in humans. Proc Natl Acad Sci USA *112*, 11678–11683.

Brookes, M.J., Tewarie, P.K., Hunt, B.A.E., Robson, S.E., Gascoyne, L.E., Liddle, E.B., Liddle, P.F., and Morris, P.G. (2016). A multi-layer network approach to MEG connectivity analysis. Neuroimage *132*, 425–438.

Buldú, J.M., and Porter, M.A. (2018). Frequency-based brain networks: From a multiplex framework to a full multilayer description. Netw. Neurosci. *2*, 418–441.

Carmon, J., Heege, J., Necus, J.H., Owen, T.W., Pipa, G., Kaiser, M., Taylor, P.N., and Wang, Y. (2020). Reliability and comparability of human brain structural covariance networks. Neuroimage *220*, 117104.

Crossley, N.A., Mechelli, A., Scott, J., Carletti, F., Fox, P.T., McGuire, P., and Bullmore, E.T. (2014). The hubs of the human connectome are generally implicated in the anatomy of brain disorders. Brain *137*, 2382–2395.

De Domenico, M. (2017). Multilayer modeling and analysis of human brain networks. Gigascience *6*, 1–8.

De Domenico, M., Sasai, S., and Arenas, A. (2016). Mapping multiplex hubs in human functional brain networks. Front. Neurosci. *10*, 326.

Dimitriadis, S.I. (2021). Reconfiguration of αmplitude driven dominant coupling modes (DoCM) mediated by α-band in adolescents with schizophrenia spectrum disorders. Prog Neuropsychopharmacol Biol Psychiatry *108*, 110073.

Dimitriadis, S.I., Zouridakis, G., Rezaie, R., Babajani-Feremi, A., and Papanicolaou, A.C. (2015). Functional connectivity changes detected with magnetoencephalography after mild traumatic brain injury. Neuroimage Clin. *9*, 519–531.

Dimitriadis, S.I., Antonakakis, M., Simos, P., Fletcher, J.M., and Papanicolaou, A.C. (2017a). Data-Driven Topological Filtering Based on Orthogonal Minimal Spanning Trees: Application to Multigroup Magnetoencephalography Resting-State Connectivity. Brain Connect. *7*, 661–670.

Dimitriadis, S.I., Salis, C., Tarnanas, I., and Linden, D.E. (2017b). Topological Filtering of Dynamic Functional Brain Networks Unfolds Informative Chronnectomics: A Novel Data-Driven Thresholding Scheme Based on Orthogonal Minimal Spanning Trees (OMSTs). Front. Neuroinformatics *11*, 28.

Dimitriadis, S.I., Drakesmith, M., Bells, S., Parker, G.D., Linden, D.E., and Jones, D.K. (2017c). Improving the Reliability of Network Metrics in Structural Brain Networks by Integrating Different Network Weighting Strategies into a Single Graph. Front. Neurosci. *11*, 694.

Dimitriadis, S.I., López, M.E., Bruña, R., Cuesta, P., Marcos, A., Maestú, F., and Pereda, E. (2018a). How to Build a Functional Connectomic Biomarker for Mild Cognitive Impairment From Source Reconstructed MEG Resting-State Activity: The Combination of ROI Representation and Connectivity Estimator Matters. Front. Neurosci. *12*, 306.

Dimitriadis, S.I., Routley, B., Linden, D.E., and Singh, K.D. (2018b). Reliability of Static and Dynamic Network Metrics in the Resting-State: A MEG-Beamformed Connectivity Analysis. Front. Neurosci. *12*, 506.

Dimitriadis, S.I., Lancaster, T.M., Perry, G., Tansey, K.E., Jones, D.K., Singh, K.D., Zammit, S., Smith, G.D., Hall, J., O'Donovan, M.C., et al. (2021). Global Brain Flexibility During Working Memory Is Reduced in a High-Genetic-Risk Group for Schizophrenia. Biol. Psychiatry Cogn. Neurosci. Neuroimaging.

Eickhoff, S.B., Yeo, B.T.T., and Genon, S. (2018). Imaging-based parcellations of the human brain. Nat. Rev. Neurosci. *19*, 672–686.

Eickhoff, S., Nichols, T.E., Van Horn, J.D., and Turner, J.A. (2016). Sharing the wealth: Neuroimaging data repositories. Neuroimage *124*, 1065–1068.

Fornito, A., Zalesky, A., and Breakspear, M. (2015). The connectomics of brain disorders. Nat. Rev. Neurosci. *16*, 159–172.

Garcés, P., Pereda, E., Hernández-Tamames, J.A., Del-Pozo, F., Maestú, F., and Pineda-Pardo, J.Á. (2016). Multimodal description of whole brain connectivity: A comparison of resting state MEG, fMRI, and DWI. Hum. Brain Mapp. *37*, 20–34.

Gifford, G., Crossley, N., Kempton, M.J., Morgan, S., Dazzan, P., Young, J., and McGuire, P. (2020). Resting state fMRI based multilayer network configuration in patients with schizophrenia. Neuroimage Clin. *25*, 102169.

Golestani, A.M., Chang, C., Kwinta, J.B., Khatamian, Y.B., and Jean Chen, J. (2015). Mapping the end-tidal CO2 response function in the resting-state BOLD fMRI signal: spatial specificity, test-retest reliability and effect of fMRI sampling rate. Neuroimage *104*, 266–277.

Guillon, J., Attal, Y., Colliot, O., La Corte, V., Dubois, B., Schwartz, D., Chavez, M., and De Vico Fallani, F. (2017). Loss of brain inter-frequency hubs in Alzheimer's disease. Sci. Rep. *7*, 10879.

Hallquist, M.N., and Hillary, F.G. (2019). Graph theory approaches to functional network organization in brain disorders: A critique for a brave new small-world. Netw. Neurosci. *3*, 1–26.

Hindriks, R., Adhikari, M.H., Murayama, Y., Ganzetti, M., Mantini, D., Logothetis, N.K., and Deco, G. (2016). Can sliding-window correlations reveal dynamic functional connectivity in resting-state fMRI? Neuroimage *127*, 242–256.

Hocke, L.M., Tong, Y., Lindsey, K.P., and de B Frederick, B. (2016). Comparison of peripheral near-infrared spectroscopy low-frequency oscillations to other denoising methods in resting state functional MRI with ultrahigh temporal resolution. Magn. Reson. Med. *76*, 1697–1707.

Joseph, A.C., Joseph, S.E., and Chen, G. (2014). Cross-border portfolio investment networks and indicators for financial crises. Sci. Rep. *4*, 3991.

Kalcher, K., Boubela, R.N., Huf, W., Bartova, L., Kronnerwetter, C., Derntl, B., Pezawas, L., Filzmoser, P., Nasel, C., and Moser, E. (2014). The spectral diversity of resting-state fluctuations in the human brain. PLoS ONE *9*, e93375.

Korhonen, O., Zanin, M., and Papo, D. (2021). Principles and open questions in functional brain network reconstruction. Hum. Brain Mapp. *42*, 3680–3711.

Laumann, T.O., Snyder, A.Z., Mitra, A., Gordon, E.M., Gratton, C., Adeyemo, B., Gilmore, A.W., Nelson, S.M., Berg, J.J., Greene, D.J., et al. (2017). On the Stability of BOLD fMRI Correlations. Cereb. Cortex *27*, 4719–4732.

Loued-Khenissi, L., Döll, O., and Preuschoff, K. (2018). An overview of functional magnetic resonance imaging techniques for organizational research. Organizational Research Methods *22*, 109442811880263.

Luppi, A.I., and Stamatakis, E.A. (2021). Combining network topology and information theory to construct representative brain networks. Netw. Neurosci. *5*, 96–124.

Lv, H., Wang, Z., Tong, E., Williams, L.M., Zaharchuk, G., Zeineh, M., Goldstein-Piekarski, A.N., Ball, T.M., Liao, C., and Wintermark, M. (2018). Resting-State Functional MRI: Everything That Nonexperts Have Always Wanted to Know. AJNR Am J Neuroradiol *39*, 1390–1399.

Mark, C.I., Mazerolle, E.L., and Chen, J.J. (2015). Metabolic and vascular origins of the BOLD effect: Implications for imaging pathology and resting-state brain function. J. Magn. Reson. Imaging *42*, 231–246.

Maturana-Candelas, A., Gómez, C., Poza, J., Pinto, N., and Hornero, R. (2019). EEG

characterization of the alzheimer's disease continuum by means of multiscale entropies. Entropy *21*, 544.

Messaritaki, E., Dimitriadis, S.I., and Jones, D.K. (2019). Optimization of graph construction can significantly increase the power of structural brain network studies. Neuroimage *199*, 495–511.

Mišić, B., and Sporns, O. (2016). From regions to connections and networks: new bridges between brain and behavior. Curr. Opin. Neurobiol. *40*, 1–7.

Muldoon, S.F., and Bassett, D.S. (2016). Network and multilayer network approaches to understanding human brain dynamics. Philos. Sci. *83*, 710–720.

Naro, A., Maggio, M.G., Leo, A., and Calabrò, R.S. (2021). Multiplex and Multilayer Network EEG Analyses: A Novel Strategy in the Differential Diagnosis of Patients with Chronic Disorders of Consciousness. Int. J. Neural Syst. *31*, 2050052.

Nikolaou, F., Orphanidou, C., Papakyriakou, P., Murphy, K., Wise, R.G., and Mitsis, G.D. (2016). Spontaneous physiological variability modulates dynamic functional connectivity in resting-state functional magnetic resonance imaging. Philos. Transact. A Math. Phys. Eng. Sci. *374*.

Noble, S., Spann, M.N., Tokoglu, F., Shen, X., Constable, R.T., and Scheinost, D. (2017). Influences on the Test-Retest Reliability of Functional Connectivity MRI and its Relationship with Behavioral Utility. Cereb. Cortex *27*, 5415–5429.

Noble, S., Scheinost, D., and Constable, R.T. (2019). A decade of test-retest reliability of functional connectivity: A systematic review and meta-analysis. Neuroimage *203*, 116157.

Parkes, L., Satterthwaite, T.D., and Bassett, D.S. (2020). Towards precise resting-state fMRI biomarkers in psychiatry: synthesizing developments in transdiagnostic research, dimensional models of psychopathology, and normative neurodevelopment. Curr. Opin. Neurobiol. *65*, 120–128.

Pereda, E., Quiroga, R.Q., and Bhattacharya, J. (2005). Nonlinear multivariate analysis of neurophysiological signals. Prog. Neurobiol. *77*, 1–37.

Poldrack, R.A., Laumann, T.O., Koyejo, O., Gregory, B., Hover, A., Chen, M.-Y., Gorgolewski, K.J., Luci, J., Joo, S.J., Boyd, R.L., et al. (2015). Long-term neural and physiological phenotyping of a single human. Nat. Commun. *6*, 8885.

Prichard, D., and Theiler, J. (1994). Generating surrogate data for time series with several simultaneously measured variables. Phys. Rev. Lett. *73*, 951–954.

Pusil, S., López, M.E., Cuesta, P., Bruña, R., Pereda, E., and Maestú, F. (2019). Hypersynchronization in mild cognitive impairment: the "X" model. Brain *142*, 3936–3950.

Rubinov, M., and Sporns, O. (2010). Complex network measures of brain connectivity: uses and interpretations. Neuroimage *52*, 1059–1069.

Savva, A.D., Mitsis, G.D., and Matsopoulos, G.K. (2019). Assessment of dynamic functional connectivity in resting-state fMRI using the sliding window technique. Brain Behav. *9*, e01255.

Schreiber, T., and Schmitz, A. (2000). Surrogate time series. Physica D: Nonlinear Phenomena *142*, 346–382.

Smith, S.M., Nichols, T.E., Vidaurre, D., Winkler, A.M., Behrens, T.E.J., Glasser, M.F.,

Ugurbil, K., Barch, D.M., Van Essen, D.C., and Miller, K.L. (2015). A positive-negative mode of population covariation links brain connectivity, demographics and behavior. Nat. Neurosci. *18*, 1565–1567.

Somandepalli, K., Kelly, C., Reiss, P.T., Zuo, X.-N., Craddock, R.C., Yan, C.-G., Petkova, E., Castellanos, F.X., Milham, M.P., and Di Martino, A. (2015). Short-term test-retest reliability of resting state fMRI metrics in children with and without attention-deficit/hyperactivity disorder. Dev. Cogn. Neurosci. *15*, 83–93.

Song, J., Desphande, A.S., Meier, T.B., Tudorascu, D.L., Vergun, S., Nair, V.A., Biswal, B.B., Meyerand, M.E., Birn, R.M., Bellec, P., et al. (2012). Age-related differences in test-retest reliability in resting-state brain functional connectivity. PLoS ONE *7*, e49847.

Sporns, O. (2011). Networks of the Brain (MIT).

Sporns, O. (2014). Contributions and challenges for network models in cognitive neuroscience. Nat. Neurosci. *17*, 652–660.

Sporns, O., and Betzel, R.F. (2016). Modular Brain Networks. Annu. Rev. Psychol. *67*, 613–640.

Stam, C.J. (2014). Modern network science of neurological disorders. Nat. Rev. Neurosci. *15*, 683–695.

Székely, G.J., and Rizzo, M.L. (2013). The distance correlation-test of independence in high dimension. J. Multivar. Anal. *117*, 193–213.

Termenon, M., Jaillard, A., Delon-Martin, C., and Achard, S. (2016). Reliability of graph analysis of resting state fMRI using test-retest dataset from the Human Connectome Project. Neuroimage *142*, 172–187.

Tewarie, P., Hillebrand, A., van Dijk, B.W., Stam, C.J., O'Neill, G.C., Van Mieghem, P., Meier, J.M., Woolrich, M.W., Morris, P.G., and Brookes, M.J. (2016). Integrating cross-frequency and within band functional networks in resting-state MEG: A multi-layer network approach. Neuroimage *142*, 324–336.

Theiler, J., Eubank, S., Longtin, A., Galdrikian, B., and Doyne Farmer, J. (1992). Testing for nonlinearity in time series: the method of surrogate data. Physica D: Nonlinear Phenomena *58*, 77–94.

Tulay, E.E., Metin, B., Tarhan, N., and Arıkan, M.K. (2019). Multimodal neuroimaging: basic concepts and classification of neuropsychiatric diseases. Clin. EEG Neurosci. *50*, 20–33.

Van Dijk, K.R.A., Hedden, T., Venkataraman, A., Evans, K.C., Lazar, S.W., and Buckner, R.L. (2010). Intrinsic functional connectivity as a tool for human connectomics: theory, properties, and optimization. J. Neurophysiol. *103*, 297–321.

Van Mieghem, P. (2016). Interconnectivity structure of a general interdependent network. Phys. Rev. E *93*, 042305.

Wang, J.-H., Zuo, X.-N., Gohel, S., Milham, M.P., Biswal, B.B., and He, Y. (2011). Graph theoretical analysis of functional brain networks: test-retest evaluation on short- and long-term resting-state functional MRI data. PLoS ONE *6*, e21976.

Wang, J., Ren, Y., Hu, X., Nguyen, V.T., Guo, L., Han, J., and Guo, C.C. (2017). Test-retest reliability of functional connectivity networks during naturalistic fMRI paradigms. Hum. Brain Mapp. *38*, 2226–2241.

Williamson, B.J., De Domenico, M., and Kadis, D.S. (2021). Multilayer connector hub mapping reveals key brain regions supporting expressive language. Brain Connect. *11*, 45–55.

Yuen, N.H., Osachoff, N., and Chen, J.J. (2019). Intrinsic Frequencies of the Resting-State fMRI Signal: The Frequency Dependence of Functional Connectivity and the Effect of Mode Mixing. Front. Neurosci. *13*, 900.

Yu, M., Engels, M.M.A., Hillebrand, A., van Straaten, E.C.W., Gouw, A.A., Teunissen, C., van der Flier, W.M., Scheltens, P., and Stam, C.J. (2017). Selective impairment of hippocampus and posterior hub areas in Alzheimer's disease: an MEG-based multiplex network study. Brain *140*, 1466–1485.

Zalesky, A., Fornito, A., Cocchi, L., Gollo, L.L., and Breakspear, M. (2014). Time-resolved resting-state brain networks. Proc Natl Acad Sci USA *111*, 10341–10346.

Zhang, Z., Telesford, Q.K., Giusti, C., Lim, K.O., and Bassett, D.S. (2016). Choosing wavelet methods, filters, and lengths for functional brain network construction. PLoS ONE *11*, e0157243.

Oscillatory hyperactivity and hyperconnectivity in young APOE-□4 carriers and hypoconnectivity in Alzheimer's disease | eLife.

New Introduction to Multiple Time Series Analysis | SpringerLink.